

Degradation of resolution in a homogeneous dual-readout hadronic calorimeter

Donald E. Groom

Lawrence Berkeley National Laboratory, 50R6008, Berkeley, CA 94720, USA

Abstract

If the scintillator response to a hadronic shower in a semi-infinite uniform calorimeter structure is S relative to the electronic response, then $S/E = [f_{em} + (1 - f_{em})(h/e)]$, where E is the incident hadron energy, f_{em} is the electronic shower fraction, and h/e is the hadron/electron response ratio. If there is also a simultaneous readout with a different h/e , say a Cherenkov signal C , then a linear combination of the two signals provides an estimator of E that is proportional to the incident energy and whose distribution is nearly Gaussian—even though the S and C distributions are non-linear in E , wide, and skewed. Since an estimator of f_{em} is also obtained, it is no longer a stochastic variable. Much of the remaining resolution variance is due to sampling fluctuations. These can be avoided in a homogeneous calorimeter. The energy resolution depends upon the contrast in h/e between the two channels. h/e is small in the Cherenkov channel. *Mechanisms that increase h/e in sampling calorimeters with organic scintillator readout are not available in a homogeneous inorganic scintillator calorimeter.* The h/e contrast is very likely too small to provide the needed energy resolution.

Keywords: Hadronic calorimetry, hadron cascades, sampling calorimetry

PACS: 02.70.Uu, 29.40.Ka, 29.40.Mc, 29.40Vj, 34.50.Bw

1. Introduction

A homogeneous dual-readout hadron calorimeter has been suggested for possible use at a future linear collider [1]. The machine will probably be an e^+e^- collider and in some concepts will have a long bunch spacing ($\mathcal{O}(100\text{ ns})$), so that detectors with time constants in this range might be used. Discrimination between the Cherenkov signal (C) and scintillator (S) optical signals is expected to use a combination of timing, color, and, possibly, Cherenkov light direction and polarization.

In practice corrections must be made for cracks, leakage, and light collection variations, and the structure usually varies with depth. For the purposes of

Email address: degroom@lbl.gov (Donald E. Groom)

this analysis we shall assume that the corrections have been made properly, and consider a semi-infinite calorimeter with uniform structure that is either fine-sampling or homogeneous.

In each high-energy interaction in a hadronic cascade an average of 1/4 of the energy is carried away by π^0 's [2]. These immediately decay to γ 's which initiate electromagnetic (EM) showers. This occurs many times, with the result that a large fraction f_{em} of the incident energy joins the EM shower. The mean, $\langle f_{em} \rangle$, is ≈ 0.5 for 100–150 GeV incident pions. It increases slowly with incident energy E , asymptotically approaching unity.

The hadronic response S to an incident hadron with energy E (calibrated to electron response) is

$$S = E[f_{em} + (1 - f_{em})(h/e)] . \quad (1)$$

The EM energy deposit is detected with relative efficiency e , and the hadronic signal with relative efficiency h . Both vary from event to event. In part because of low multiplicities in the initial hadronic interactions, the variance of h is much larger than the variance of e . It makes sense to treat h/e as a stochastic variable. To the extent that the variance of h dominates, the distribution of the conventional e/h is not useful. In Sec. 5 we treat the distribution of h/e as Gaussian.

Most energy deposit is by very low-energy electrons and charged hadrons. Because so many generations are involved in a high-energy cascade, the hadron spectra are essentially independent of the cascade's origin except for overall normalization. This “universal spectrum” concept is discussed in detail in Ref. [2]. It is because of this feature that $\langle h/e \rangle$ is a robust quantity, independent of energy and incident hadron species.

The energy-independent $\langle h/e \rangle$ does depend upon calorimeter composition and structure, as well as the readout—for example, an organic scintillator readout is sensitive to the otherwise-invisible neutron content of the cascade while a Cherenkov readout is relatively blind to the hadronic content. $\langle f_{em} \rangle$ can be found by fitting the average π^-/e response as a function of test-beam energy with an appropriate $\langle f_{em} \rangle$ parameterization such as a power law in energy [2].¹

Usually $\langle h/e \rangle$ is less than unity, since the EM contribution is detected with greater efficiency than the hadronic energy deposition. If $\langle h/e \rangle$ is not unity, then the broad, skewed f_{em} probability distribution function (p.d.f.) significantly degrades and skews the energy resolution, resulting in the familiar wide, non-Gaussian energy distributions. The response is not linear with energy because of the energy dependence of $\langle f_{em} \rangle$. If f_{em} could be *measured* for each event, then the response as given in Eq. 1 could be corrected to the actual energy with a nearly Gaussian distribution and a mean proportional to the energy.

¹Technically, a power-law fit finds $a = (1 - \langle h/e \rangle)E_0^{1-m}$. Since $1 - m$ is small and the scale energy E_0 is close to 1 GeV for pion-induced cascades, the distinction is minor: $\langle h/e \rangle \approx 1 - a$. A similar distinction occurs when other parameterizations are used. $\langle h/e \rangle$ itself cannot be isolated.

The importance of measuring the EM content on an event-by-event basis was realized as early as 1980, although how to use the information was not so clear. There was even a (stillborn) dual readout test by A. Erwin (BNL) using scintillator and radiator plates [3].

EM showers result in large local energy deposit; with sufficient readout segmentation this “lumpiness” provides a measure of f_{em} . Weighting this part differently than the remaining signal might improve resolution. This approach was used with some success by the WA1 collaboration [4], but has been less successful elsewhere, e.g., for the ATLAS central barrel calorimeter [5].

In a 1983 summer school review of high-energy calorimetry, P. Mockett stressed the importance of measuring the fractional EM content of the shower. He speculated that one could use two sampling media, an electron-sensitive detector (Cherenkov) and an ionization sensitive detector (scintillator). He also imagined taking advantage of the fast Cherenkov pulse and slow scintillation signal in a heavy inorganic scintillator. Both suggestions were prophetic [6].

Such a separation was actually made by Theodosiou et al. [7] in 1984, using the time structure of pulses observed in scintillating glass. He thought the technique might permit electron/hadron separation or even help with particle identification. Winn later suggested using color in addition to timing to make the separation [8]. There must have been considerable speculation about dual-readout calorimetry, but only Theodosiou et al. took this speculation into the laboratory.

Part of the problem was that the physics of energy deposition had not yet been elucidated, or at least widely understood. This came in the late 1980s with the work of Fabjan et al. [9], Wigmans [10], Brückmann et al. [11], Drews et al. [12], and others, but a key element was the energy deposition inventories produced by the very detailed simulations of Gabriel and his collaborators at Oak Ridge as early as 1974 [9, 13].

Much of the hadronic energy resolution problem was related to the large fraction of missing energy in the hadronic sector, due to nuclear dissociation, nuclear recoil, residual nuclear excitation, μ and ν escape, and (unobserved) neutrons. Scintillator response to highly ionizing charged particles is non-linear, resulting in significantly more lost signal. For a time it was thought that ionization by U fission products could make up some of the lost energy [9, 10, 14], but non-linear scintillator response to the highly ionizing fragments negated most of the gains.

In a sampling calorimeter, only a small fraction of the energy is deposited in the sensors (quartz or scintillator), and fluctuations in this fraction are more important than intrinsic fluctuations in the hadronic signal. These dominate, once f_{em} is removed. The sampling fluctuations are avoided in a homogeneous calorimeter. The possibly long bunch spacing at a future linear collider opens the door to a homogeneous dual-readout dense crystal or glass calorimeter, where a fast, blue, Cherenkov pulse might be separated from a slower, redder scintillation signal. Crystal studies are being successfully explored by Akchurin, et al. [15–22], but with only speculative mention of dual-readout hadron calorimeters. A feasibility study is part of a new proposal [23].

Akchurin et al. have demonstrated signal separation that would be adequate

for recovering energy estimators that are linear in the corrected energy and have a nearly Gaussian distribution. However, I am concerned that the energy *resolution* would not be adequate. In this paper I explore the likely resolution as a function of energy and $\langle h/e|_S \rangle$ using resolution contributions based on published crystal, glass, and sampling calorimeter performance. Simple, transparent Monte Carlo simulations (MC's) are used by choice, to make the physics more transparent than if a sophisticated MC such as GEANT4 were used. The p.d.f. of f_{em} is approximated with some care, while other resolution contributions are taken to be Gaussian.

2. $\langle h/e \rangle$ in a high-density crystal or glass scintillator

In an EM cascade the electrons are relativistic until their energies fall well below the critical energy, so that almost all of the energy is deposited by near-minimum ionizing electrons. No appreciable energy exits from the EM cascade via photonuclear interactions. The result is a response very nearly linear in the incident electron or photon energy.

Hadronic interactions deposit energy in a variety of ways. (An inventory is given in Table 1 [by Gabriel and Schmidt] in Ref. [9], and detailed discussions can be found in Refs. [24–26] and other recent reviews). A large fraction of the hadronic energy ($\approx 20\%$ for Fe/scintillator and $\approx 40\%$ for U/scintillator sampling calorimeters) goes to nuclear dissociation and recoil, and is “invisible.” Neutrinos and most muons escape. Some fraction of the neutrons can be detected via $n-p$ scattering in hydrogenous materials such as organic scintillator, but much or most of the neutron energy is also lost. Low-energy protons and charged fission fragments produce saturated signals in scintillator. (This occurs in inorganic [27] as well as organic scintillators [28].) All of these factors result in low visible response to the hadronic component of the cascade relative to response to the EM component.

Detection of recoil protons in neutron scattering in hydrogenous detectors increases h [29]. In a sampling calorimeter a disproportionate fraction of the EM energy is deposited in the higher- Z absorber; the absorber/active region thickness ratio can be “tuned” to decrease e . Both of these effects increase h/e . In practical sampling calorimeters $\langle h/e \rangle$ is typically 0.7, and can be made to approach unity with careful design.

Neither mechanism for increasing h/e is available to a high-density homogeneous calorimeter.

As we shall see, the resolution is dependent on the “ h/e contrast,” the difference between $\langle h/e \rangle$ for the Cherenkov ($\langle h/e|_C \rangle$) and scintillation ($\langle h/e|_S \rangle$) readouts. Based on experience with quartz-fiber readout calorimeters [30–32], $\langle h/e|_C \rangle = 0.20\text{--}0.25$.² There are few data concerning $\langle h/e|_S \rangle$ in a homogeneous calorimeter, but there is no way to hide EM energy in the absorber and there is

²From the data shown in Table 3 of Ref. [30] I obtain $h/e|_C = 0.247$ [35].

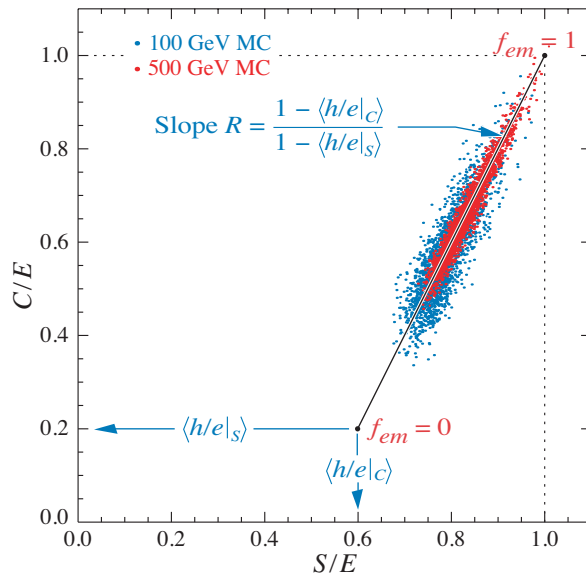


Figure 1: Energy-independent event locus in the C/E - S/E plane. As indicated by the MC events, resolution improves and the mean moves upward along the locus as the beam energy is increased.

very little neutron sensitivity. We might expect as much as 30% of the hadron energy to be expended on nuclear dissociation and therefore invisible, and 15%–20% to be carried by neutrons. These alone would result in $\langle h/e|_S \rangle \approx 0.5$. There are other effects, such as incomplete Cherenkov-scintillator separation and saturated scintillator response to highly ionizing particles, so $\langle h/e|_S \rangle = 0.35$ – 0.5 might be expected. This is corroborated by a comment in Ref. [16]: “The e/h value of ECAL [PbWO_4] as a scintillation device is much larger than for the Cu/plastic sampling structure in DREAM: 2.4 vs. 1.3.” ($h/e = 0.43$ vs 0.7 .)

3. Dual-readout hadronic calorimetry

In 1997 Wigmans discussed the advantages of adding a quartz-fiber readout to the scintillator readout of a sampling calorimeter [33]. With a Cherenkov readout (C) fairly blind to hadronic activity and a scintillator readout (S) with optimized hadronic response, f_{em} could be determined (or eliminated) and a corrected energy found. The DREAM collaboration elegantly implemented this proposal with a test-beam calorimeter having quartz and plastic scintillator fibers in copper tubes [31, 32, 34].

In the dual-readout case Eq. 1 is replaced by [31, 35–37]

$$S = E[f_{em} + (1 - f_{em})(h/e|_S)] \quad (2)$$

$$C = E[f_{em} + (1 - f_{em})(h/e_C)] \quad (3)$$

In parametric form, Eqns. (2) and (3) describe a straight line-segment event locus in the C - S (or C/E - S/E) plane, as illustrated in Fig. 1. If the cascade is “all electromagnetic” ($f_{em} = 1$), then $S/E = C/E = 1$. If the cascade is “all hadronic” ($f_{em} = 0$), then $S/E = h/e|_S$ and $C/E = h/e|_C$. (The MC “events” shown in the figure are discussed below.) The slope in the C/E - S/E plane is independent of energy; with increasing energy the distribution just moves up along the locus.

It is convenient to introduce the less cumbersome notation $h/e|_X \equiv \eta_X$:

$$S = E[f_{em} + (1 - f_{em})\eta_S] \quad (4)$$

$$C = E[f_{em} + (1 - f_{em})\eta_C] \quad (5)$$

Equations (4) and (5), linear in $1/E$ and f_{em} , can be rewritten as

$$\begin{pmatrix} S & -(1 - \eta_S) \\ C & -(1 - \eta_C) \end{pmatrix} \begin{pmatrix} 1/E \\ f_{em} \end{pmatrix} = \begin{pmatrix} \eta_S \\ \eta_C \end{pmatrix} \quad (6)$$

with solutions [37]

$$E = \frac{S(1 - \eta_C) - C(1 - \eta_S)}{\eta_S - \eta_C} \quad (7)$$

$$f_{em} = \frac{C\eta_S - S\eta_C}{S(1 - \eta_C) - C(1 - \eta_S)}. \quad (8)$$

There is an important difference between Eqs. 1, 2, and 4, and Eq. 7: The first three give estimators of the scintillator response, given f_{em} , η_S , and the incident energy E . In contrast, Eq. 7 provides an *estimator* of this energy given S , C , η_S and η_C . Similarly, Eq. 8 provides an *estimator* of f_{em} .

The sensitivity of the energy estimator to the h/e contrast is particularly manifest in Eq. 7: If $\langle \eta_S \rangle - \langle \eta_C \rangle$ is small compared to the statistical fluctuations of η_S and η_C , then the scatter in the energy estimators will be large.

In Eqs. 7 and 8, η_C and η_S are the values *peculiar to that event*. These are unknown—and unknowable, until some way of tagging the hadronic composition becomes available.³ But in an experimental situation, an estimator of the energy must be established for each event. There is little choice but to replace these quantities by their means.

In this case, it is convenient to write the energy estimator (Eq. 7) more compactly as [35–37]

$$E = \frac{RS - C}{R - 1}, \quad (9)$$

where I have made use of the slope of the event locus (the ratio of ranges of S and C) shown in Fig. 1:

$$R \equiv \frac{1 - \langle \eta_C \rangle}{1 - \langle \eta_S \rangle} \quad (10)$$

³Neutron detection has been proposed and is being explored for this purpose [38, 39].

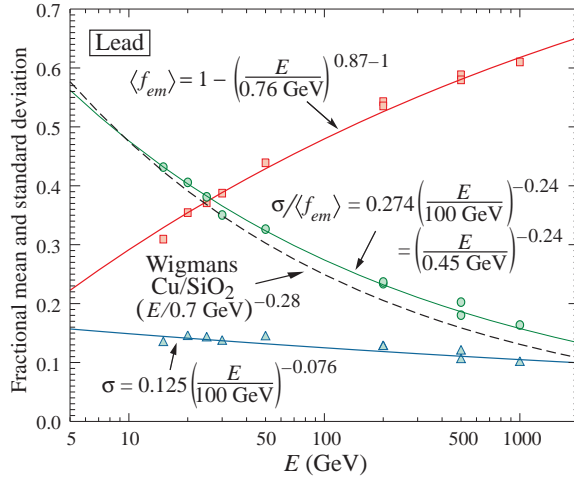


Figure 2: The mean, standard deviation, and fractional standard deviation of f_{em} in lead, as simulated by FLUKA90. This is basically Fig. 3(b) in Ref. [35]. An error in the fit to the fractional standard deviation has been corrected, a slightly different MC data set has been used, and Wigmans' fit to the fractional standard deviation in a copper/quartz-fiber calorimeter has been added [24].

4. Electromagnetic fraction

In a dual-readout calorimeter estimators of E and f_{em} can be determined on an event-by-event basis. The EM fraction f_{em} is no longer a stochastic variable.

The f_{em} p.d.f. has an energy-dependent mean (near 0.5 at 100–150 GeV, approaching unity as $E \rightarrow \infty$). Its standard deviation is about 11%, depending weakly on energy and calorimeter composition, and it is skewed to the large- f_{em} side [24, 35]. The mean, fractional standard deviation, and standard deviation of f_{em} as simulated by FLUKA90⁴ for cascades in a large lead cylinder are shown in Fig. 2. For this case I obtain the empirical fits

$$\langle f_{em} \rangle = 1 - \left(\frac{E}{0.76 \text{ GeV}} \right)^{0.87-1} \quad (11)$$

$$\sigma = 0.125 \left(\frac{E}{100 \text{ GeV}} \right)^{-0.076} . \quad (12)$$

(The functional form of Eq. 11 satisfies the requirement $\langle f_{em} \rangle \rightarrow 1$ as $E \rightarrow \infty$, and σ must slowly approach 0 as $E \rightarrow \infty$.) Although I use these expressions for the present calculations, the numerical constants will be somewhat different for different calorimeter structures. The fractional standard deviation found for

⁴Since FLUKA90 many improvements have been made, especially in the nuclear physics modeling. The high-energy cascade modeling is nearly the same. Only the π^0 energy fraction in the cascade is of interest here.

a copper/quartz-fiber calorimeter (Fig. 4.46 in Ref. [24]) is shown in Fig. 2 for comparison.

Values of f_{em} must be chosen from distributions with the means and r.m.s. widths given by Eqs. 11 and 12, and with skewness that agrees with the detailed hadronic cascade simulations. This dimensionless skewness γ_1 ($= \mu_3/\sigma^3$, where μ_3 is the third moment about the mean) is not well-determined from our simulations, but it is about 0.6, which I assume here. Any smooth positive function bounded between 0 and 1 that can be adjusted to have these properties would be satisfactory. I have found it convenient to use the Beta function

$$B(x; \alpha, \beta) \propto x^{\alpha-1}(1-x)^{\beta-1}, \quad (13)$$

with α and β adjusted to obtain the desired σ and γ_1 . It is then displaced so that its mean is $\langle f_{em} \rangle$. The displaced function does not quite go to zero at $x = 1$, but it is sufficiently close to zero that the problem can be ignored. The procedure is illustrated in Fig. 3(a) for $E = 200$ GeV pions in lead. The distribution from the FLUKA simulation is superimposed.

Values of f_{em} are chosen from this function by choosing uniformly distributed random points (f_{em}, y) and retaining the values of f_{em} where y is not above the p.d.f. at that value of f_{em} . A histogram of one such array of values is overlaid on the model p.d.f. in Fig. 3(b).

Experimental distributions of f_{em} obtained with the DREAM detector are shown in Refs. [31], [32], and [33]. Because of resolution effects they are considerably broader and less skewed than the FLUKA-generated distributions. The typical f_{em} estimator distribution shown in Fig. 3(b) illustrates the resolution loss.

5. Resolution contributions

In a dual-readout calorimeter f_{em} has been elevated from a stochastic quantity to a measured quantity. In the absence of other resolution contributions, C and S are completely correlated, and the reconstructed energy distribution given by Eq. (7) or Eq. (9) is a delta function.

The signal distribution is broadened by photoelectron (p.e.) statistics, uncertain shower leakage corrections, uncorrected signal collection irregularities, electronic noise, sampling fluctuations (in the case of a sampling calorimeter), intrinsic fluctuations in the visible fraction of hadronic energy deposition, and other effects. As a matter of convenience in this discussion, I ignore the contributions from the readout-associated factors or assume that their contributions are lumped into $\sigma^{\text{p.e.}}$. Although published resolution measurements often involve constants and other deviations from $1/\sqrt{E}$ scaling, for our present purposes I use

$$\frac{\sigma_E}{E} = \frac{\sigma^{\text{p.e.}}}{\sqrt{E}} \oplus \frac{\sigma^{\text{intr}}}{\sqrt{E}} \oplus \frac{\sigma^{\text{samp}}}{\sqrt{E}}, \quad (14)$$

where the σ 's on the right side are fractional resolutions at 1 GeV if E is in GeV. The hadronic intrinsic and sampling contributions (σ^{intr} and σ^{samp}) are discussed below.

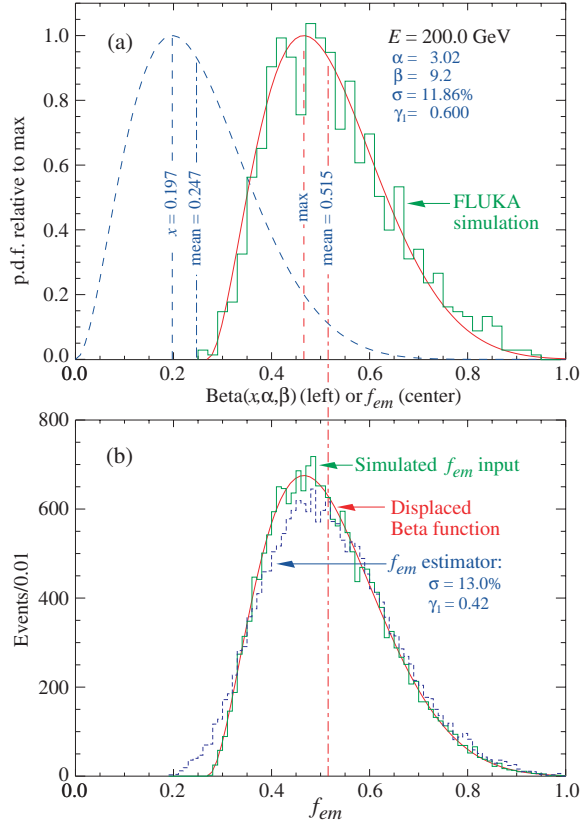


Figure 3: Approximation of the f_{em} p.d.f. by a displaced Beta p.d.f. for 200 GeV pions incident on a lead “calorimeter.” (a) The Beta p.d.f. (dashed curve) with σ from Eq. 12 and $\gamma_1 = 0.6$, and the distribution displaced to the mean given by Eq. 11 (solid curve). The superimposed histogram is from a FLUKA90 simulation. (b) A histogram of 20 000 MC values chosen from this p.d.f., compared with the displaced Beta function. The dashed histogram shows the corresponding f_{em} estimator distribution obtained via Eq. 8 for the case $\langle \eta_C \rangle = 0.25$ and $\langle \eta_S \rangle = 0.50$. It is broader and less skewed than the input distribution.

The nuclear dissociation energy deposit distribution is distinctly non-Gaussian; for example, see Fig. 4 in Ref. [33]. But visible energy deposit via ionization by charged particles is more important in materials of interest, and its distribution is not completely correlated with that of nuclear dissociation and other missing energy. The resulting visible energy deposit distribution in compensated sampling calorimeters seems to be near-Gaussian, and Drews et al. [12] assume Gaussian distributions in separating intrinsic and sampling contributions. Gaussian distributions are assumed in Eq. 14 and elsewhere in this analysis.

1. *Readout statistics.* Photomultipliers or avalanche photodiodes will likely be used to detect the scintillation and Cherenkov light. In this case Gaussian (Poisson) fluctuations with variance equal to the number of detected photons, and hence proportional to the energy, are added to the signals. The fractional uncertainty thus scales as $1/\sqrt{E}$.

Electromagnetic calorimeters provide guidance about obtainable resolution. Some of these are tabulated in Sec. 28.9.1 of Ref. [36]. Although fractional resolution as good as $2\%/\sqrt{E}$ has been obtained in scintillating crystal calorimeters, the best reported Cherenkov response in lead-glass EM calorimeters was 5%, for the OPAL endcap [40], corresponding to 400 p.e.'s/GeV. To maximize the number of photoelectrons collected, $\approx 45\%$ of the ends of the lead-glass blocks were covered by the PMT's. Such collection efficiency will probably not be possible with the proposed crystal calorimeter.

At the other extreme, the DREAM detector obtained $35\%/\sqrt{E}$ (8 p.e./GeV) with quartz fibers [41–43]. Improving Cherenkov light yield has been a major goal of the collaboration's recent work with a variety of crystals [15–22]. Yields as high as 55 p.e./GeV have been reported for Mo-doped PbWO_4 [21]. Further improvements are possible, for example by extending the UV response of the photodetectors and UV transmission of the radiators.

In this model study it is realistic to assume a middle ground, $\sigma_C^{\text{p.e.}} = \sigma_{0,C}^{\text{p.e.}}/\sqrt{C}$, where $\sigma_{0,C}^{\text{p.e.}} \approx 10\text{--}20\%$, or 100–25 p.e.'s/GeV. In most of the MC's reported here, 15%, or 44 p.e.'s/GeV was used.

In most of the dual-readout homogeneous calorimeters under discussion, the Cherenkov and scintillator signals are to be separated by color and pulse shape. This requires that the scintillation signal is not large compared with the Cherenkov signal, say $\langle S \rangle = \xi^2 \langle C \rangle$, where ξ^2 is “a few.” We take $\xi^2 = 4$ in this study: $\sigma_{0,S}^{\text{p.e.}} = \sigma_{0,C}^{\text{p.e.}}/\xi$.

2. *Sampling and intrinsic fluctuations.* In a sampling calorimeter most of the energy is deposited in the absorber, and there are large fluctuations in the small fraction of the visible hadronic energy deposited in the active medium. A homogeneous calorimeter is not subject to these sampling fluctuations; in fact, this is an important reason for choosing it.⁵

⁵Some suggested schemes, such as alternating lead glass Cherenkov planes with heavy glass scintillator planes [44], are totally active but only quasi-homogeneous. In these cases sampling fluctuations have some importance.

Table 1: Examples of near-compensating sampling hadron calorimeters. For our present purposes some calorimeter structure variation and constant terms in the fitted resolution have been ignored.

Calorimeter	Passive	Active	Resolution	h/e	Reference
(Akesson et al.)	Cu, U/Cu, U	Scint (2.5mm)	$36\%/ \sqrt{E}$	0.90	[45]
HELIOS	U (3 mm)	Scint (2.5 mm)	$34\%/ \sqrt{E}$	0.984 ± 0.006	[46]
ZEUS FCAL	U (3.0/3.2 mm)	Scint (2,5/3.0 mm)	$35\%/ \sqrt{E}$	1.03	[47, 48]
WA80	U (3 mm)	Scint (3 mm)	$67\%/ \sqrt{E}$	0.89	[49]
(Drews, et al.)	<i>Pb (10 mm)</i>	<i>Scint (2.5 mm)</i>	<i>$44\%/ \sqrt{E}$</i>	<i>0.90 ± 0.01</i>	[12, 50]
(Drews, et al.)	U (3.2 mm)	Scint (3.0 mm)	$36\%/ \sqrt{E}$	0.99 ± 0.01	[12]
SPACAL	Pb (4× scint vol)	1 mm scint fibers	$30\%/ \sqrt{E}$	0.87	[51, 52]
PCAL*	Pb†(10 mm)	Scint (3 mm)	$32\%/ \sqrt{E}$	0.89	[53]

* $E \leq 6.8$ GeV.

† Every 6th plate is 16 mm thick Fe.

Much of the hadronic energy deposit is invisible, going to nuclear disassociation, the production of unseen neutrons, etc., with consequent “intrinsic” fluctuations in the visible signal even if there is no absorber. In all but a few dedicated test-beam experiments, sampling and intrinsic fluctuations are inextricable. Drews et al. [12] studied the problem using compensated sandwich calorimeters with separate readouts for odd- and even- numbered layers. Since sampling fluctuations from layer to layer are independent, the *sum* of the odd- and even-layer signals, and their *difference* have the same variance. Signals from the intrinsic fluctuations are correlated between layers, so sums and differences could be used to separate sampling and intrinsic variances. ($\sigma^{\text{p.e.}} \approx 7\%/ \sqrt{E}$ did not significantly broaden the responses.) In the case of lead plates, the sampling contribution was $(41.2 \pm 0.9)\%/ \sqrt{E}$ and the intrinsic contribution was $(13.4 \pm 4.7)\%/ \sqrt{E}$. In the case of uranium plates, the sampling contribution was $(31.1 \pm 0.9)\%/ \sqrt{E}$ and the intrinsic contribution was $(20.4 \pm 2.4)\%/ \sqrt{E}$. Lead is probably closest to compositions likely to be considered for the homogeneous calorimeter, so this result is relevant to the present discussion.

Since f_{em} fluctuations do not contribute in a compensating calorimeter (by definition of “compensating”), its resolution is the result of p.e., sampling, and intrinsic variations.⁶ Examples of near-compensating calorimeter resolution are shown in Table 1. We may take $\sigma_E = 35\%/ \sqrt{E}$ as a representative “best case.” Drew et al.’s Pb-plate calorimeter achieved $44\%/ \sqrt{E}$ (italicized line in Table 1).

⁶This is not quite true. Suppose, for example, that $\langle h/e \rangle = 1$, and we select a subset of events for which h/e fluctuates to 10% below the mean, to 0.9. For these events S is sensitive to fluctuations of f_{em} . The *distribution* of h/e about unity thus introduces sensitivity to f_{em} .

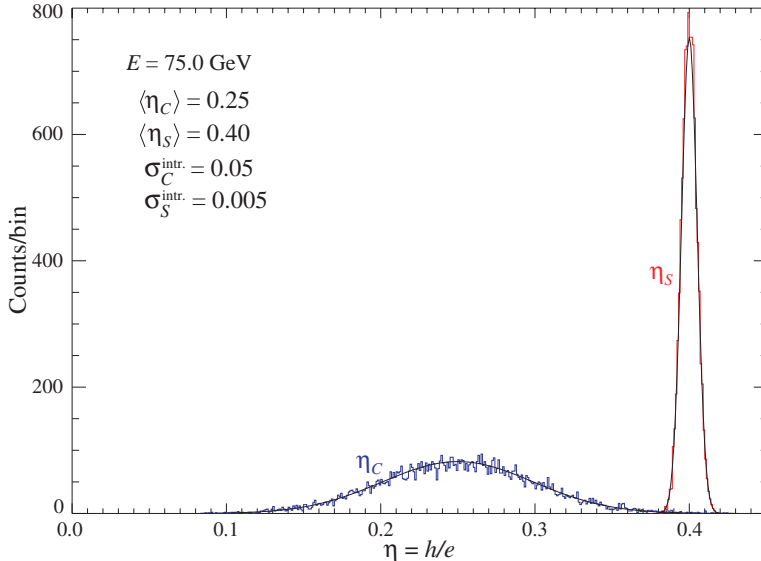


Figure 4: Input p.d.f.'s and MC realizations of the h/e distributions at 75 GeV for $\langle\eta_C\rangle = 0.25$ and $\langle\eta_S\rangle = 0.40$. $\sigma_S^{\text{intr.}}$ and $\sigma_C^{\text{intr.}}$ are from Table 2.

Scaling to this resolution, $\sigma_S^{\text{intr.}} \approx (35/44) \times 13.4\%/\sqrt{E} \approx 11\%/\sqrt{E}$. We adopt this as the fiducial scintillator intrinsic resolution for this study. If $\langle\eta_S\rangle \neq 1$, then $\sigma_S^{\text{intr.}} = 0.11 \langle\eta_S\rangle/\sqrt{E}$.

The standard deviation $\sigma_C^{\text{intr.}}$ of η_C is more problematic. Light produced by relativistic pions, with smaller contributions from other hadrons and electrons produced via nuclear γ -ray interactions, contribute a hadronic component to the Cherenkov response. The QFCAL [30] and DREAM [32] collaborations found $\langle\eta_C\rangle = 0.20$ – 0.25 . Since most of the scintillation signal is produced by nonrelativistic ionizing particles, η_S and η_C are nearly independent.

Typically about 35 (relativistic) π^\pm 's are produced by a 100 GeV pion showering in Pb.⁷ The fractional standard deviation is $1/\sqrt{35} = 0.17$ at 100 GeV, or $1.7/\sqrt{E}$. This broad distribution is scaled down by $\langle\eta_C\rangle = 0.20$ – 0.25 : $\sigma_C^{\text{intr.}} \approx 1.7 \langle\eta_C\rangle/\sqrt{E}$.

These results are summarized in Table 2. Typical distributions of η_S and η_C are shown in Fig. 4. Since the energy distributions reported for compensating calorimeter, e.g., as given in Table 1 are all consistent with Gaussian distribution, it is evidently valid to consider the distributions discussed in this section as Gaussian as well. This results in near-Gaussian energy-estimator distributions as reconstructed from S and C .

⁷Section 2.3.1.3 of Ref. [24].

Table 2: Summary of resolution contributions. Reference values in the last column are used in Sec. 6.

Std dev	Value at E	Reference value	Optimistic value
$\sigma_C^{\text{p.e.}}$	$\sigma_{0,C}^{\text{p.e.}}/\sqrt{C}$	$\sigma_{0,C}^{\text{p.e.}} = 15\%$	$\sigma_{0,C}^{\text{p.e.}} = 5\%$
$\sigma_S^{\text{p.e.}}$	$\sigma_{0,C}^{\text{p.e.}}/\xi\sqrt{S}$	$\xi = 2$	$\xi = 10$
$\sigma_C^{\text{intr.}}$	$\sigma_{0,C}^{\text{intr.}} \langle \eta_C \rangle / \sqrt{E}$	$\sigma_{0,C}^{\text{intr.}} = 170\%$	$\sigma_{0,C}^{\text{intr.}} = 85\%$
$\sigma_S^{\text{intr.}}$	$\sigma_{0,S}^{\text{intr.}} \langle \eta_S \rangle / \sqrt{E}$	$\sigma_{0,S}^{\text{intr.}} = 11\%$	5.5%

6. Simulation of the energy estimator distribution

Equation 9 and the equivalent Eq. 7 describe the estimator of incident pion energy as obtained from the observed scintillation and Cherenkov signals. We incorporate the resolution contributions discussed in Sec. 5 and summarized in Table 2 to obtain distributions of S , C , and the energy estimator E via a simple, transparent Monte Carlo calculation as follows:

1. Choose the incident energy E and the detection efficiency ratios $\langle \eta_S \rangle$ and $\langle \eta_C \rangle$, fixing the latter in the range 0.20–0.25.
2. Choose the resolution parameters, using the reference values given in Table 2.
3. Generate an array of N values of f_{em} chosen from the displaced Beta distribution for energy E .
4. Generate N values of η_S from a normal distribution with mean $\langle \eta_S \rangle$ and fractional standard deviation $\sigma_S^{\text{intr.}}$. Similarly, generate N values of η_C from a normal distribution with mean $\langle \eta_C \rangle$ and standard deviation $\sigma_C^{\text{intr.}}$.
5. Construct the corresponding S and C arrays via Eqs. 4 and 5.
6. Replace each S and C as calculated in step 4 with values chosen from normal distributions with means S and C and standard deviations $\sigma_{0,C}^{\text{p.e.}}\sqrt{C}$ and $\sigma_{0,S}^{\text{p.e.}}\sqrt{S}$, respectively. The resulting S and C include p.e. statistics, and are used for subsequent “data analysis.” (Since $\sigma_{0,C}^{\text{p.e.}}/\sqrt{C}$ and $\sigma_{0,S}^{\text{p.e.}}/\sqrt{S}$ are fractional standard deviations, $\sigma_{0,C}^{\text{p.e.}}\sqrt{C}$ and $\sigma_{0,S}^{\text{p.e.}}\sqrt{S}$ have the same units as S and C (GeV).)
7. Find the energy estimator array via Eq. 7 or Eq. 9.

The results of four 10000 event simulations are shown in Fig. 5, at 75 and 200 GeV using realistic (0.4) and optimistic (0.6) values of η_S . In each case the mean value of the estimator of E (E_{est}) scaled by the beam energy is 1.00. The distributions agree well with the Gaussians with the same mean and standard deviation drawn over the E histograms. In nearly all cases $|\gamma_1| \leq 0.05$.

The fractional standard deviation of the energy estimator scales as $1/\sqrt{E}$. The coefficient (resolution at 1 GeV) as a function of $h/e|_S$ ($\equiv \eta_S$) is shown in Fig. 6 for two values of $h/e|_C$ ($\equiv \eta_C$) that bracket the range found for quartz-fiber readout calorimeters [30–32].

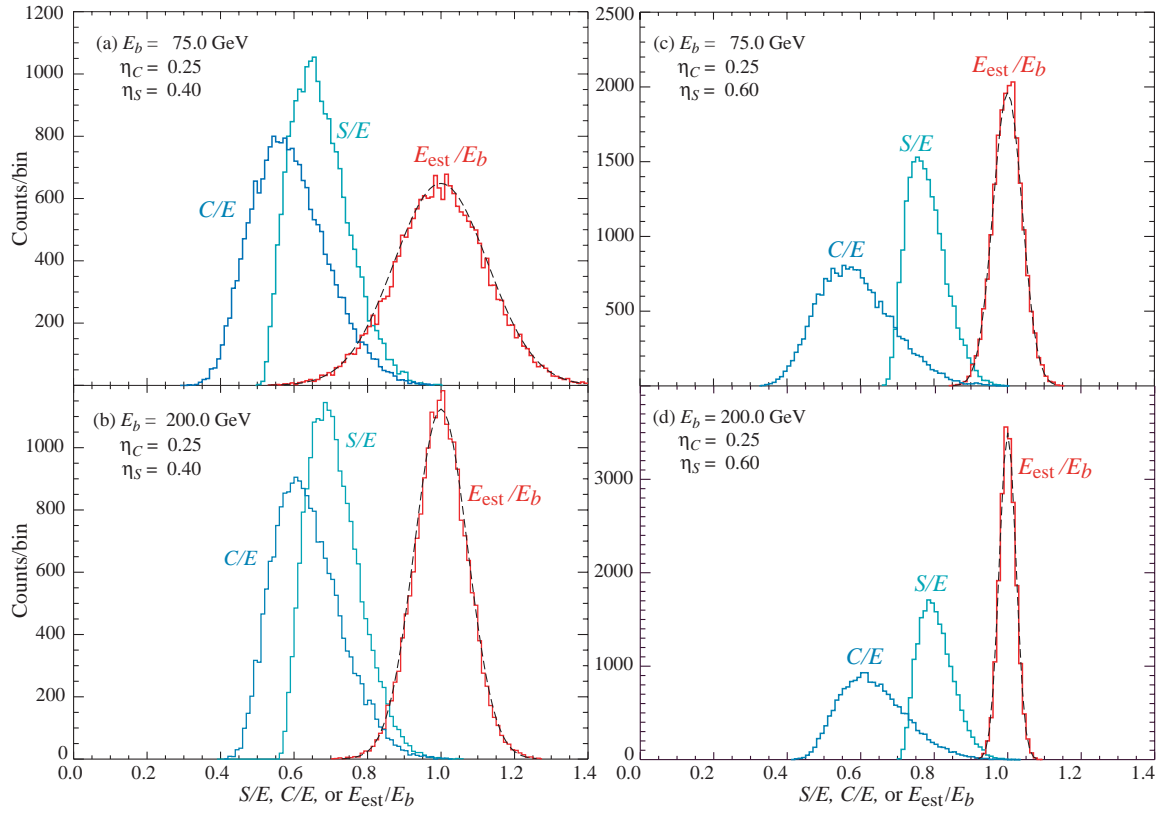


Figure 5: Monte Carlo distributions of C , S , and the estimator of E . (a) and (c) are for beam energies of 75 GeV; for (b) and (d) the beam energy is 200 GeV. For (a) and (b) $\eta_S = 0.40$, while for (c) and (d) $\eta_S = 0.60$. In all cases $\eta_C = 0.25$. Gaussians with the “measured” σ_E and mean relative to beam energy are shown as dotted black lines. Details are given in Table 3.

Table 3: Parameters for the examples shown in Fig. 5, each based on 20 000 simulated events. In all cases $\eta_C = 0.25$.

	(a)	(b)	(c)	(d)
E_b	75 GeV	200 GeV	75 GeV	200 GeV
η_S	0.40	0.40	0.60	0.60
$\langle S/E_b \rangle$	0.67	0.71	0.78	0.81
σ_S	11.6%	10.1%	6.7%	5.9%
γ_{1S}	0.57	0.62	0.58	0.59
$\langle C/E_b \rangle$	0.59	0.64	0.59	0.64
σ_C	17.2%	14.2%	17.2%	14.2%
γ_{1C}	0.42	0.55	0.45	0.53
$\langle E_{\text{est}}/E_b \rangle$	0.999	1.000	1.000	1.000
σ_E	12.8%	7.24%	3.96%	2.27%
σ_E @ 1 GeV	111.%	102.%	34.3%	32.1%
γ_{1E}	0.008	0.002	-0.015	-0.003

7. Discussion and conclusions

The standard deviations described in this section are highly uncertain, and can be used only as guides. The effect of large changes in the input variances on the resolution curves shown in Fig. 6 have been studied. Examples of optimistic excursions from best estimates are given in Table 2. At $\langle \eta_S \rangle = 0.45$ and $\langle \eta_C \rangle = 0.20$, where $\sigma_E = 52.5\%/\sqrt{E}$, the following improvements are found:

1. Increase the Cherenkov p.e. yield by a factor of nine, from $\sigma_{0,C}^{\text{p.e.}} = 15\%$ (44 p.e.'s/GeV) to $\sigma_{0,C}^{\text{p.e.}} = 5\%$ (400 p.e.'s/GeV). The resolution improves from $52.5\%/\sqrt{E}$ to $47.1\%/\sqrt{E}$, or -5.4% —not a large improvement.
2. Increase the scintillator p.e. yield by a factor of 25 ($\xi = 2 \rightarrow \xi = 10$). The resolution improves from $52.5\%/\sqrt{E}$ to $49.0\%/\sqrt{E}$, or -3.5% . At least in this model, there is no serious penalty for using a “weak” scintillator.
3. Decrease the width of the Cherenkov intrinsic hadronic resolution at 1 GeV by a factor of two, from 170% to 85%. The former number is expected from fluctuations in the number of relativistic pions produced in the cascade, and so should be relatively dependable. However, this change produces a large improvement: $52.5\%/\sqrt{E} \rightarrow 39.1\%/\sqrt{E}$, or -13.4% . The curve for this case has been added to Fig. 6.
4. Finally, halve the width of the scintillator intrinsic hadronic resolution from $11\%/\sqrt{E}$ to $5.5\%/\sqrt{E}$. As expected, there is little effect: $52.5\%/\sqrt{E} \rightarrow 52.1\%$, or -0.4% . A substantial downward excursion of this number would be unphysical.

The overall conclusion remains and is evident from Eq. 7: in a homogeneous hadronic calorimeter with dual readouts and a non-hydrogenous scintillator,

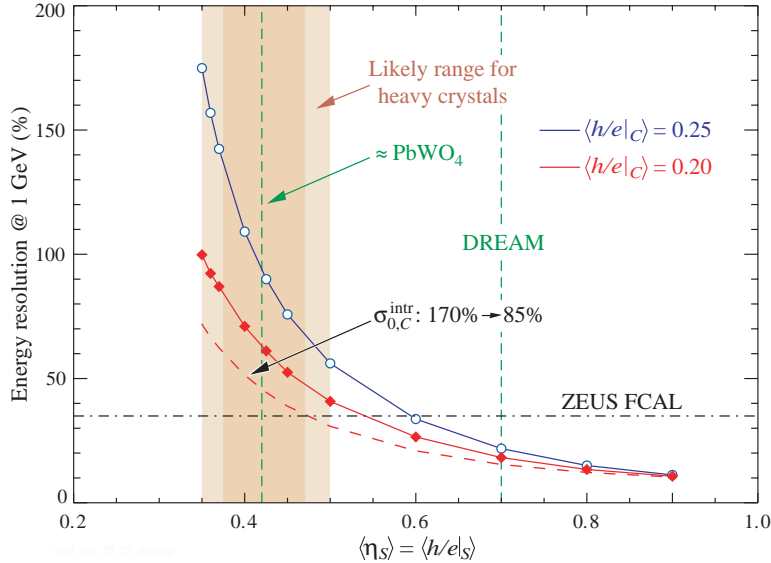


Figure 6: Dependence of resolution on η_S at two values of $\eta_C \equiv h/e|_C$. The results for $\eta_C = 0.20$ are essentially those for $\eta_C = 0.25$ displaced to the left by 0.05; it is the *contrast* between η_C and η_S that determines the resolution. The dashed line shows the effect of halving the width of the η_C p.d.f.

event-to-event fluctuations of η_C and η_S destroy the resolution if their means are close. A large contrast between them is unlikely because the mechanisms that increase $\langle \eta_S \rangle$ are not present. It remains true that the mean of the energy estimator distribution is the beam energy, and its distribution is nearly Gaussian.

Detailed simulations with a modern, sophisticated Monte Carlo program such as GEANT4 would be desirable before commitment to a large R&D effort. It would be particularly informative to understand the means and variances of η_C and η_S .

Acknowledgments

I particularly thank Adam Para for getting me interested in this problem. Richard Wigmans' book, many papers, and many personal interactions have been invaluable, as have been discussions with John Hauptman. The understanding of hadronic calorimetry underlying this paper has been slowly forged over at least the past 40 years by the insights and hard work of experts too numerous to mention.

This work was supported by the U.S. Department of Energy under Contract No. DE-AC02-05CH11231.

References

- [1] A. Para, at the NSS 2010 Workshop on Materials for Homogeneous Hadron Calorimeters, Knoxville, Tennessee (31 October 2010). The idea of a crystal homogeneous hadron calorimeter is also broached in several of the DREAM crystal studies (see esp. Ref. [19]), and feasibility studies have been proposed by the DREAM collaboration [23].
- [2] T.A. Gabriel, D.E. Groom, P.K. Job, N.V. Mokhov, G.R. Stevenson, Nuclear Instruments and Methods in Physics Research Section A 338 (1994) 336.
- [3] I am indebted to John Hauptman for his meticulous history of the subject.
- [4] H. Abramowicz, et al., Nuclear Instruments and Methods 180 (1981) 429.
- [5] V.V. Abramov, et al., Nuclear Instruments and Methods in Physics Research Section A 457 (2001) 75.
- [6] P. Mockett, A review of the physics and technology of high-energy calorimeter devices, Proceedings of 11th SLAC Summer Institute on Particle Physics, July 1983, SLAC Report No. 267 (July 1983).
- [7] G.E. Theodosiou, et al., IEEE Transactions on Nuclear Science NS-31 (1984) 57.
- [8] D. R. Winn, W. A. Worstell, IEEE Transactions on Nuclear Science 36 (1989) 334.
- [9] C.W. Fabjan, et al., Nuclear Instruments and Methods 141 (1977) 61; the energy deposition inventory in Table 1 is taken from T. A. Gabriel , W. Schmidt, ORNL/TM-5105 (1975).
- [10] R. Wigmans, Nuclear Instruments and Methods in Physics Research Section A 259 (1987) 389.
- [11] H. Brückmann, et al., Nuclear Instruments and Methods in Physics Research Section A 263 (1988) 136.
- [12] G. Drews, et al., Nuclear Instruments and Methods in Physics Research Section A 335 (1990) 335.
- [13] T. A. Gabriel & J.D. Amburgey, Nuclear Instruments and Methods 116 (1974) 333; T. A. Gabriel & W. Schmidt, Nuclear Instruments and Methods 134 (1976) 271.
- [14] C. Leroy, Y. Sirios, & R. Wigmans, Nuclear Instruments and Methods in Physics Research Section A 252 (1986) 4.
- [15] Akchurin, et al., Nuclear Instruments and Methods in Physics Research Section A 550 (2005) 185.

- [16] Akchurin, et al., Nuclear Instruments and Methods in Physics Research Section A 584 (2008) 273.
- [17] Akchurin, et al., Nuclear Instruments and Methods in Physics Research Section A 595 (2008) 359.
- [18] Akchurin, et al., Nuclear Instruments and Methods in Physics Research Section A 598 (2009) 710.
- [19] Akchurin, et al., Nuclear Instruments and Methods in Physics Research Section A 604 (2009) 512.
- [20] Akchurin, et al., Nuclear Instruments and Methods in Physics Research Section A 610 (2009) 488.
- [21] Akchurin, et al., Nuclear Instruments and Methods in Physics Research Section A 621 (2010) 212.
- [22] Akchurin, et al., Nuclear Instruments and Methods in Physics Research Section A 638 (2011) 47.
- [23] R. Wigmans, Proposal CERN-SPSC-2010-012/SPSC-M-771) (April 2010).
- [24] R. Wigmans, Calorimetry: Energy Measurement in Particle Physics, in: International Series of Monographs on Physics, vol. 107, 2000, pp. 1–726, Oxford University Press (2000).
- [25] C. Leroy, P.-G. Rancoita, Principles of Radiation Interaction in Matter and Detection, World Scientific (2004).
- [26] N. Akchurin & R. Wigmans, Nuclear Instruments and Methods in Physics Research Section A 666 (2012) 80.
- [27] W. Moses, IEEE Transactions on Nuclear Science NS-55 (2008) 1049; W. Mengesha, et al., IEEE Transactions on Nuclear Science 45 (1998) 456.
- [28] See fig 3.25, p. 145 in Ref. [24].
- [29] Y. Galaktionov, et al., Nuclear Instruments and Methods in Physics Research Section A 251 (1986) 258.
- [30] N. Akchurin, et al., Nuclear Instruments and Methods in Physics Research Section A 399 (1997) 202.
- [31] R. Wigmans, First results of the DREAM project, Proceedings of the 11th International Conference on Calorimetry in Particle Physics, Perugia, Italy, 29 March–02 April, 2004, ed. C. Cecchi, P. Cenci, P. Lumbrano, & M. Pepe, World Scientific (2005) 241.
- [32] N. Akchurin, et al., Nuclear Instruments and Methods in Physics Research Section A 537 (2005) 537.

- [33] R. Wigmans, Quartz Fibers and the Prospects for Hadron Calorimetry at the 1% Level, Proceedings of the 7th International Conference on on Calorimetry in Particle Physics, Tuscon, Arizona, 9–12 November, 1997, ed. E. Cheu, T. Embry, J. Rutherford, & R. Wigmans, World Scientific (1998) 182.
- [34] R. Wigmans, Nuclear Instruments and Methods in Physics Research Section A 572 (2007) 215.
- [35] D.E. Groom, Nuclear Instruments and Methods in Physics Research Section A 572 (2007) 633.
- [36] J. Beringer, et al. (Particle Data Group), Physical Review D 86 (2012) 010001.
- [37] D.E. Groom, Nuclear Instruments and Methods in Physics Research Section A 697 (2013) 84.
- [38] N. Akchurin, et al., Nuclear Instruments and Methods in Physics Research Section A 581 (2007) 643.
- [39] N. Akchurin, et al., Nuclear Instruments and Methods in Physics Research Section A 598 (2009) 422.
- [40] OPAL collaboration, Nuclear Instruments and Methods in Physics Research Section A 305 (1991) 275.
- [41] N. Akchurin, et al., Nuclear Instruments and Methods in Physics Research Section A 533 (2004) 305.
- [42] N. Akchurin, et al., Nuclear Instruments and Methods in Physics Research Section A 536 (2005) 29.
- [43] N. Akchurin, et al., Nuclear Instruments and Methods in Physics Research Section A 550 (2005) 185.
- [44] T. Zhao, “Active Absorber Calorimeter,” Contribution 119 at Linear Collider Workshop 2006, Bangalore, India (8–13 March 2006); indico.cern.ch/contributionDisplay.py?contribId=119,amp;sessionId=5,amp;confId=568.
- [45] T. Akesson, et al., Nuclear Instruments and Methods in Physics Research Section A 241 (1985) 17.
- [46] T. Akesson, et al., Nuclear Instruments and Methods in Physics Research Section A 262 (1987).
- [47] A. Anderson, et al., Nuclear Instruments and Methods in Physics Research Section A 309 (1991) 101.
- [48] www-zeus.desy.de/bluebook/ch05/subsection2.4.15.3.html.

- [49] G. R. Young, et al., Nuclear Instruments and Methods in Physics Research Section A 279 (1989) 503.
- [50] E. Bernardi, et al., Nuclear Instruments and Methods in Physics Research Section A 262 (1987) 229. /
- [51] D. Acosta, et al., Nuclear Instruments and Methods in Physics Research Section A 308 (1991) 481.
- [52] T. A. Armstrong, et al., Nuclear Instruments and Methods in Physics Research Section A 406 (1998) 227.
- [53] D. Fox, et al., Nuclear Instruments and Methods in Physics Research Section A 317 (1992) 474.